Mechanical Systems and Signal Processing 164 (2022) 108235

Contents lists available at ScienceDirect

Mechanical Systems and Signal Processing

journal homepage: www.elsevier.com/locate/ymssp

# Comparison of lock-in correlation and a novel periodogram method for experimental multi-harmonic thermoelastic analysis

A.J. Molina-Viedma [a,*], L. Felipe-Sesé [a], E. López-Alba [b], F.A. Díaz [b]

[a] Departamento de Ingeniería Mecánica y Minera, Campus Científico Tecnológico de Linares, Universidad de Jaén, 23700 Linares, Spain
[b] Departamento de Ingeniería Mecánica y Minera, Campus Las Lagunillas, Universidad de Jaén, 23071 Jaén, Spain

ARTICLE INFO

*Keywords:*
Thermoelasticity
Periodogram
Lock-in correlation
Multi-harmonic analysis

ABSTRACT

Lock-in correlation is a simple, efficient and widely employed method for thermoelastic stress analysis under cyclic loading. Frequency domain analysis of the thermoelastic signal using the Fourier transform has been also valuable for researchers, even though it presents some drawbacks. In this paper, a new frequency-domain method for thermoelastic analysis through periodograms using Welch's averaging method has been developed. This method supplies the lack of phase shift information of the simple Fourier transform for thermoelastic signals and considerably reduce the data size. This work evaluates its performance against lock-in correlation through two experiments with opposite features for multi-harmonic analysis. One experiment consisted in the analysis of the thermoelastic signal in a plate with a centred hole, exhibiting a stress concentration and using the second harmonic as an indicator of the non-linearities. The second experiment consisted in the characterisation of mode shapes thermal maps during the simultaneous excitation of multiple specimen resonances. In comparison with the stress concentrator experiment, here the level of the thermal signal is lower and the number of frequencies to analyse is higher. The analysis of the thermal maps by both methods revealed that they yield practically identical results for any experiment. However, the evaluation of the computation efficiency highlights that the periodogram method has fewer memory requirements whereas, in terms of computation time, lock-in correlation is more efficient to analyse fewer frequencies in short image sequence tests, being the periodogram method more efficient for the opposite case.

## 1. Introduction

Thermoelastic Stress Analysis (TSA) is a technique that exploits the thermal emission produced by elastic deformations in solids under cyclic loading [1,2] or even under random excitation [3]. For isotropic materials, provided that the load is fast enough to meet adiabatic conditions in the solid, it can be found from the first thermodynamic law that there exists a proportional relation between the temperature variation and the first invariant amplitude of the Cauchy stress tensor, that is to say, the volume change. This relation, known as thermoelastic constant, can be calibrated using a reference measurement of stresses [4,5].

Experimentally, the relation between temperature and emittance in the infrared spectrum has been exploited through optical sensors, sensitive to these wavelengths. Hence, infrared scanners [6,7] or, more recently, focal plane array infrared sensor cameras, make contactless full-field measurements possible for TSA. Methodologies using TSA with optical means have profusely arisen for

* Corresponding author.
*E-mail address:* ajmolina@ujaen.es (A.J. Molina-Viedma).

https://doi.org/10.1016/j.ymssp.2021.108235
Received 18 February 2021; Received in revised form 7 June 2021; Accepted 12 July 2021

fatigue and fracture mechanics to obtain, for instance, the stress intensity factor [8–11] or the T-stress [12], high-cycle fatigue energy analysis [13] or the investigation of damage mechanisms in composites [14]. Nonetheless, additional uses have been performed, like for material characterization [15] or modal characterisation [16].

Despite the high sensitivity of thermographic sensors, the thermoelastic signal is very subtle (a few mK in amplitude), so it is highly polluted by noise. For this reason, a filtering method has been required alongside TSA to extract the information at the frequency term of interest. The lock-in correlation has been the most popular method for TSA [17]. Its popularity comes from the simplicity of the lock-in amplifiers [2,18], whose main components are a multiplier, a low-pass filter and a DC amplifier. It only requires a reference signal to remove all the terms whose frequency is different from the reference [19]. The reference signal can be taken from a physical measurement of the load or a function generator in phase with the load. The result is just a thermogram whose pixels data can be represented as a vector whose magnitude is the amplitude of the thermoelastic signal and the phase is the phase shift between the thermal and the reference signal. However, the possibility of performing off-line lock-in by software is a recent alternative to hardware lock-in which simplifies the equipment, reducing costs and improving the portability [20].

A great variety of uses of lock-in and TSA can be found in the literature. Estrada-Estrada and Patterson [21] employed a lock-in amplifier in the experiments they conducted to study the possible path-dependency inconsistency in TSA, especially for irregular waveform loads. Chen et al. [22] used lock-in for the analysis of cracks in welded and non-welded T-joints. Grammatikos et al. [23] used it to filter the thermoelastic signal for the fatigue study of a repaired debonded composite sample. Another example on the use of lock-in was performed by Li et al. [24] in a methodology for rapid determination of the fatigue limit. Liu et al. [25] also employed it to identify components in multi-layered composites structures through thermoelastic assessment and an artificial neural network model. An alternative way to perform lock-in in the absence of a known reference signal was illustrated by Sakagami et al. [26], who employed a self-reference signal for the study of cracks evolution in steel bridges.

Nevertheless, lock-in has not been exclusively intended for the study of fracture and fatigue phenomena. Lock-in correlation has been also popular for the evaluation of stress fields in modal shapes of single resonances. In this sense, Di Renzo et al. [27] measured the normalised stress fields in a turbine blade using TSA and lock-in, as a complement to the modal analysis with scanning laser Doppler vibrometry. Fruehmann et al. [28] employed lock-in correlation to propose a methodology for the inspection of aerospace composite structures based on resonance excitation. Backman and Greene [29] employed it for mode shapes measurement of gas turbine blades.

Besides lock-in, there are other methodologies to filter the thermoelastic signal at cyclic load frequency. One of them is the employed in the commercial software IRTA, by Diagnostic Engineering Solutions, which decomposed the signal in the sum of a first-order polynomial and the sinusoid at the frequency of interest with a short number of superharmonics. De Finis et al. [30] employed it for the mechanical characterization of stainless steels. Ancona et al. [31] evaluated the Paris law in stainless steels with this method. Díaz et al. [32] also utilised it for the evaluation of the stress intensity factor in combination with the results of digital image correlation.

However, a more extended method is the Fourier transform. Using the transformation of the thermal signal to the frequency domain, the researchers identified the desired term at a specific frequency line in a more exhaustive decomposition of the original signal. Silva and Ravichandran [33,34] used the Fourier transform to extract the thermoelastic signal to perform TSA and 2D digital image correlation simultaneously with a single camera. Gamot et al. [5] employed the Fourier transform in their study of a calibration method of TSA from DIC data based on the mode I stress intensity factor. Pitarresi et al. [35] proposed a methodology in which the loading frequency is firstly retrieved using the Fourier transform of one point of the thermal map and afterwards the off-line lock-in correlation was performed to obtain the thermoelastic map. In a recent study, Molina-Viedma et al. [16] also employed the Fourier transform to evaluate the capabilities of thermography to obtain thermal fields of modal shapes at higher frequencies than the employed in classical fatigue and fracture analyses.

As an off-line method, Fourier transform also contributes to the simplification of the experimental equipment. However, it does not perform any correlation with a reference signal, so the phase shift between excitation and response will not be obtained if needed. Moreover, when the thermoelastic signal is weak and large sequences are required, the outcome of the Fourier transform is an additional dataset which is, at least, half the size of the original image sequence, as long as the one-sided spectrum is used. That means various gigabytes of the dataset's size that makes it difficult to deal with. An alternative to Fourier transform that carries the phase shift information regarding a reference signal and reduce significantly the dataset size is to employ an averaging method for the cross-power spectrum between thermal and reference signals. To the author's knowledge, this has not been performed yet.

In this study, a viable alternative to Fourier transform to obtain true-amplitude and phase shift of the thermoelastic signal is proposed. It is based on the periodogram Welch's averaging method [36] using the cross-power spectrum. The purpose of the study is to evaluate and compare lock-in correlation and this method. To illustrate the capabilities of both methods for any situation, the multi-harmonic analysis of two common experiments in mechanical engineering was performed for the evaluation of multiple frequency terms occurring simultaneously in the signal. First, the analysis of the stress concentration in a flat steel sample due to a hole was performed, evaluating also the second harmonic as indicator of the presence of non-linearities. Second, the thermoelastic behaviour of a plate under multiple simultaneous resonances has been also performed. This is a very representative experiment to illustrate the capabilities of the methods for multi-harmonic analysis providing different and independent maps, which are associated with the thermal fields of the modal shapes. In both tests, the lock-in and the periodogram methods were performed to filter the thermal signals at the frequencies of interest under identical conditions. The results from both methods were compared, highlighting their respective advantages and disadvantages according to the parameters required in the tests. This comparison also includes the computational efficiency of the methods through the evaluation of the computation time after multiple executions on the same dataset and RAM consumption.

## 2. Processing methods

### 2.1. Periodogram averaging method

From a signal $y$ with $N$ samples in the time domain, its Fourier transform is obtained as follows:

$$Y(n) = \frac{1}{N}\sum_{j=0}^{N-1} y(j) e^{-i\left(\frac{2\pi jn}{N}\right)} \qquad n = 0, 1, \cdots, N-1 \tag{1}$$

As can be observed, the length of the transform is also $N$. When working with vision systems, even for not very long signals, the number of sensors corresponding to the pixels in the images is huge. That means to store an additional large dataset that might be hard to handle in memory. This is especially inefficient when just a few frequencies are being analysed.

Averaging the spectrum of correlative segments of the signal is commonly employed for diverse signal analyses. It reduces the resulting length of the vector $Y$ proportionally to the length ratio between the segment and the full signal, maintaining the spectral information of the whole sequence. Nevertheless, the Fourier transform of the segments cannot be averaged as cancellation occurs. In this case, the arbitrary phase of the frequencies of analysis in all the segments makes a stationary frequency term tend to zero after averaging several segments, as illustrated in Fig. 1. Hence, the actual amplitude would not be obtained, or even identified.

The use of power spectra estimations through peridograms avoids the cancellation. The Welch's averaging method, which calculates the periodograms via Fourier transform [36], is the best known. This method averages the spectrum of segments with equal length. It also allows employing overlapped segments, which helps to exploit the information contained in the signal. Hence, let $y$ be a signal with $N$ samples. This signal is divided into segments of length $L$ with $P$ samples overlapped so that there are $K$ segments $y_1(j)$, $\cdots, y_K(j)$ with $j = 0, 1, \cdots, L-1$. It is illustrated in Fig. 2. The Fourier transform in eq. (1) of each segment can then be calculated as follows, modified by a selected window $w(j)$:

$$Y_k^{'}(n) = \frac{1}{L}\sum_{j=0}^{L-1} y_k(j) w(j) e^{-i\left(\frac{2\pi jn}{L}\right)} \qquad k = 1, 2, \cdots, K \tag{2}$$

Nevertheless, for subsequent analysis, the one-sided spectrum of the Fourier Transform will be used:

$$Y_k(n) = 2Y_k^{'}(n) \tag{3}$$

Where $n = 0, 1, \cdots, L/2$ if $L$ is even or $n = 0, 1, \cdots, (L-1)/2$ when odd, reducing the size of the spectrum without loss of information. However, it is usually given as a function of the vector of frequency lines in Hertz, $f$, knowing the relation $f = nf_s/L$, where $f_s$ is the sampling frequency. Then, the modified periodogram of each segment, $P_{YY_k}$, presented as the one-sided spectrum, is:

$$P_{YYk}(f) = \frac{L}{U}\frac{|Y_k(f)|^2}{2}$$

$$U = \frac{1}{L}\sum_{j=0}^{L-1} w^2(j) \tag{4}$$

Where $U$ is the scaling factor of the applied window. Therefore, the power spectrum of the whole signal is the average of the $K$ periodograms:

$$\widehat{P}_{YY}(f) = \frac{1}{K}\sum_{k=1}^{K} P_{YYk}(f) \tag{5}$$

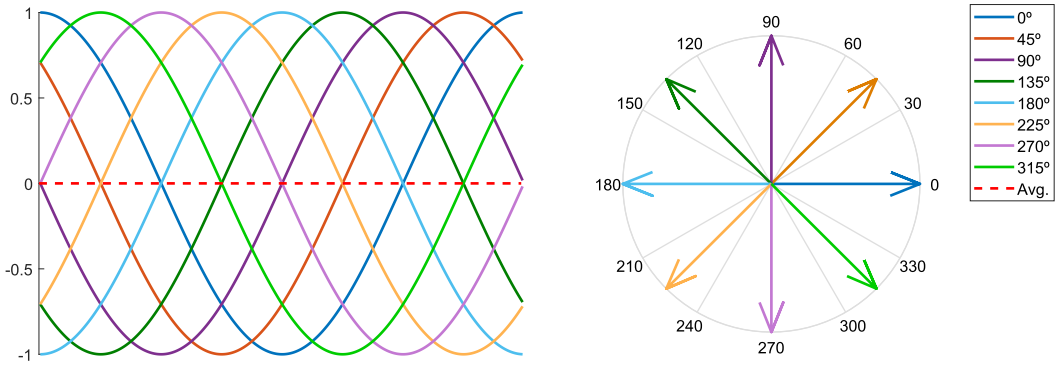


**Fig. 1.** Signal cancellation when averaging multiple segments with equal amplitude and a homogenous distribution of the initial phase.

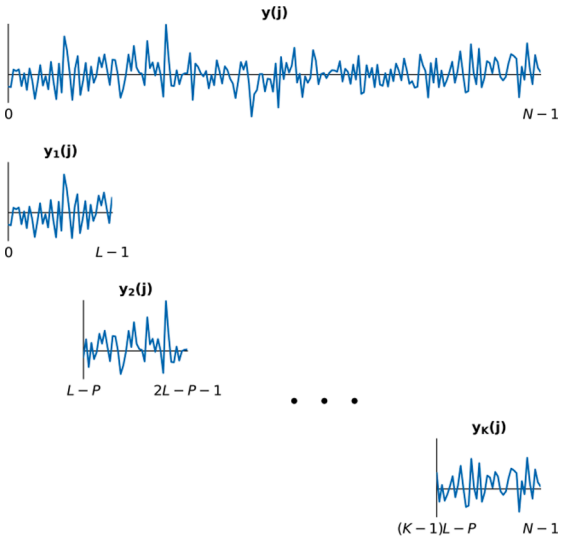


**Fig. 2.** Segmentation of the full-length signal to estimate the averaged power spectrum.

The result in eq. (5) is proportional to the square amplitude of every frequency line but no information about the phase-shift is given. The cross-power spectrum between the response signal, $Y$, and a reference signal, $X$, provides the required solution. Analogous to the auto-power spectrum estimation in eq. (4), the cross-power spectrum of each segment of the signal, $P_{XYk}$, and the resulting averaged one, $\widehat{P}_{XY}$, can be obtained as follows:

$$P_{XYk}(f) = \frac{L}{U}\frac{X_k^*(f)Y_k(f)}{2}$$

$$\widehat{P}_{XY}(f) = \frac{1}{K}\sum_{k=1}^{K} P_{XYk}(f) \tag{6}$$

Here, the superscript * represents the conjugate. The phase of the cross-power spectrum is the difference of phase between signal $Y$ and $X$ , which is stable for the principal frequency terms contained in the signal. Likewise, the noise terms are reduced during the averaging.

To obtain the real magnitude of the signal from the averaged cross-power spectrum, it is necessary to remove the amplitude of the reference signal. First, consider that if every frequency of interest coincides with a frequency line in the spectrum, i.e., with any value of $f$, no window is needed to avoid leakage in the signal. That means to use a flat window $w(j) = 1$ so that $U = L$. Therefore, the amplitude of the reference signal can be calculated from the power spectrum as follows, according to Eq. (4):

$$\left|\widehat{X}_k(f)\right| = \sqrt{2\widehat{P}_{XXk}(f)} \tag{7}$$

From this equation and eq. (6) using the same parameters during the calculation of the periodograms, it can be obtained:

$$\widehat{Y}_k(f) = \frac{2\widehat{P}_{XY}(f)}{\left|\widehat{X}_k(f)\right|} \tag{8}$$

The result is the averaged transform of the signal, $y$, in the frequency domain using overlap between segments of $L$ lines. The length of this one-sided spectrum is equal to half the length of the segments, $L/2$, instead of half the length of the full signal, $N/2$. Despite the size is reduced, it contains the lines of interest. For non arbitrarily large signals, an overlap of one half of the segment, $P = L/2$, is recommended to reduce the variance [36].

Finally, both a measured reference signal from any transducer or an artificial signal created on purpose can be employed. For thermal images, every pixel represents a sensor so eq. (8) can be defined as a function of pixel's coordinates as $\widehat{Y}_k(p_{col}, p_{row}, f)$.

### 2.2. Off-line lock-in

Since on-line lock-in, using an amplifier, is not possible when multiple frequencies must be analysed at a time, off-line lock-in can be employed as a software approach based on Fourier series. According to this, the signal can be decomposed as sines at the discrete frequencies $f_n = nf_s/N$, according to the sampling frequency, $f_s$, and the number of samples, $N$, with $n = 0, \cdots, N/2$ when N is even, which is the most common in practice. Using the subscript $Y$ to indicate the frequency of interest, the signal can be decomposed as

follows:

$$y(j) = A_Y \sin\left(2\pi f_Y t_j + \phi_Y\right) + \sum_{n=0}^{N/2} (1 - \delta_{nY}) A_n \sin\left(2\pi f_n t_j + \phi_n\right)$$

$$t_j = \frac{j}{f_s} \qquad j = 0, 1, \cdots, N-1$$

$$\delta_{nY} = \begin{cases} 1 & n = Y \\ 0 & n \neq Y \end{cases} \tag{9}$$

Where $A$ and $\phi$ represent the amplitude and phase of each term. Now, consider a reference monotonic signal, $x$, and its quadrature, $x^{'}$:

$$x(j) = 2\sin\left(2\pi f_X \frac{j}{f_s} + \phi_X\right)$$

$$x^{'}(j) = 2\cos\left(2\pi f_X \frac{j}{f_s} + \phi_X\right) \tag{10}$$

If $f_X = f_Y$ and the signal $y$ is multiplied by each of these reference signals, the following is obtained:

$$y \cdot x = A_Y \left[\cos\Delta\phi - \cos\left(4\pi f_Y \frac{j}{f_s} + \phi_Y + \phi_X\right)\right] + \sum_{n=0}^{L/2} \left[(1 - \delta_{nY}) A_n \sin\left(2\pi f_n \frac{j}{f_s} + \phi_n\right) x\right]$$

$$y \cdot x^{'} = A_Y \left[\sin\Delta\phi + \sin\left(4\pi f_Y \frac{j}{f_s} + \phi_Y + \phi_X\right)\right] + \sum_{n=0}^{L/2} \left[(1 - \delta_{nY}) A_n \sin\left(2\pi f_n \frac{j}{f_s} + \phi_n\right) x^{'}\right] \tag{11}$$

From these operations, all the terms of the signal are modulated by the frequency $f_Y$. The most relevant result of this modulation for this analysis is that the DC term only depends on the amplitude of the signal, $A_Y$, and the phase shift, $\Delta\phi$, at the frequency of interest. Besides, this term can be obtained from both modulated signals as the mean value for the $N$ values of the whole sequence so that:

$$R = \frac{1}{N} \sum_{j=0}^{N-1} y(j) x(j) = A_Y \cos\Delta\phi$$

$$I = \frac{1}{N} \sum_{j=0}^{N-1} y(j) x^{'}(j) = A_Y \sin\Delta\phi \tag{12}$$

From which the amplitude and phase shift can be obtained:

$$A_Y = \sqrt{R^2 + I^2}$$

$$\Delta\phi = \operatorname{atan}\frac{I}{R} \tag{13}$$

It must be noted that lock-in correlation and the Fourier transform are mathematically equivalent. Hence, the result of eq. (12) is the real and the imaginary parts of the specific frequency $f_Y$ in eq (1). For coding simplicity, lock-in should be programmed using eq. (1).

When this process is performed at every pixel signal, an image of amplitude $A_Y(p_{col}, p_{row})$ and phase shift $\Delta\phi(p_{col}, p_{row})$ is obtained for the frequency of interest. Using complex algebra, a complex image is obtained, with $R$ and $I$ as the real and imaginary parts, respectively, which is equivalent to the averaged transform $\widehat{Y}_k(p_{col}, p_{row}, f_Y)$, using the periodogram averaging method. This method can be considered simpler and more efficient than periodograms, particularly for a single-frequency analysis. However, when a multi-harmonic analysis is performed, the reference signal containing multiple frequencies of interest must not be employed as all these terms will be mixed at the DC term. Therefore, the off-line locking processing must be performed as many times as the number of frequencies of interests. The reference signals must be synthetically created on purpose for each one. The phase of the reference signal, $\phi_X$, may be arbitrarily chosen when the phase shift is only employed to resolve the sign of the signal at the different points of the specimen. In that case, it can be set to 0 for simplicity. When the precise shift with the reference signal is required, the phase of the reference signal may be previously identified through the Fourier transform. To ensure that the frequencies of interest are in the Fourier series, the length of the signal $N$ must be such that the signal contains an integer number of cycles of these frequencies.

## 3. Experimental procedure

To evaluate the capabilities of the lock-in correlation and the periodogram averaging method for the multi-harmonic analysis of

thermal fields, two representative tests with different experimental conditions and purposes were performed: the identification of non-linear behaviour in a stress concentrator and the analysis of several mode shapes. The particularities of each experiment offered the chance to compare the capabilities of both methods for a different number of frequencies of interest and sequence length.

In both experiments, an infrared camera model FLIR X6581sc was employed to monitor the thermal emission on the samples' surface during the solicitations. This camera performs a calibration known as CNUC, which is a non-linear multi-parameter modelling of the non-uniformity behaviour of the read-only integrated circuit and allows for flexible integration time adjustments without a classical non-uniformity correction. It was provided with a 50 mm focal length lens. This camera can reach a frame rate of 303 fps at full resolution (640 × 512). The object was considered as a greybody, and the temperature was computed according to the Stefan-Boltzmann law for the radiated energy of a blackbody, $W_{bb}$:

$$W_{gb} = \varepsilon W_{bb} = \varepsilon \sigma T^4$$

Where $\varepsilon$ is the emissivity of the surface. The rest of the total radiation received is due to reflection from ambient sources. The emission of the atmosphere was considered negligible. The emissivity of the specimens' surface was increased up to 0.95 by applying a black mate paint coating. The reduced reflections of the ambient infrared radiation were characterised by the reflected temperature, measured on a diffuse reflective surface. Its value was 296.4 K, similar to ambient temperature.

Finally, the thermal images were processed employing the described methods using an in-house Pythoń s program to return the thermal field at the required frequencies by inputting the recorded thermal sequences.

### 3.1. Stress concentration

In the first experiment, the methods were employed to identify the thermoelastic effect and non-linearities in a stress concentration problem under axial load. The sample was a thin steel plate of section 30 × 2 mm, with a central hole of 10 mm in diameter for stress concentration. It was loaded with a sine cyclic monotonic load of an average load of 11,000 N and 1000 N in amplitude at 10 Hz so that plasticity was locally reached close to the hole at the peak load and distorted the thermal signal. This was performed in an MTS Landmark servohydraulic testing machine, with a maximum dynamic load capacity of 25 kN.

The IR camera was placed in front of the plate, as shown in Fig. 3 (a). The field of view was cropped, fitting the central part of the sample to reduce the processing time. That yielded a final frame size 322 × 64 pixels. 3000 frames of the loading event were recorded with a frame rate of 300 fps and an integration time of 1000 μs.

For this particular case, the reference signal was created by software. The non-linear effects are the focus of this test since they involve a distortion in the sinusoidal signal that generates superharmonics of the fundamental frequency. Therefore, lock-in correlation was performed twice with a mono-harmonic signal at both the load frequency (10 Hz) and its second harmonic (20 Hz). The employed recording parameters guaranteed that the full sequence contained an integer number of cycles at these frequencies. For the periodogram averaging method, this signal consisted in the sum of two sine function at those two frequencies. 300 images per segment and 150 samples of overlap were employed in this method. With this length, the original time-domain thermal signal is reduced to a spectrum of 151 lines from 0 to 150 Hz with a frequency resolution of 1 Hz, according to the method's description. In this way, the correlated frequencies coincided with a frequency line and, as stated in Section 2.1., no anti-leakage window is required. For both methods, the reference signals used the same initial phase, zero, to keep the same phase shift.

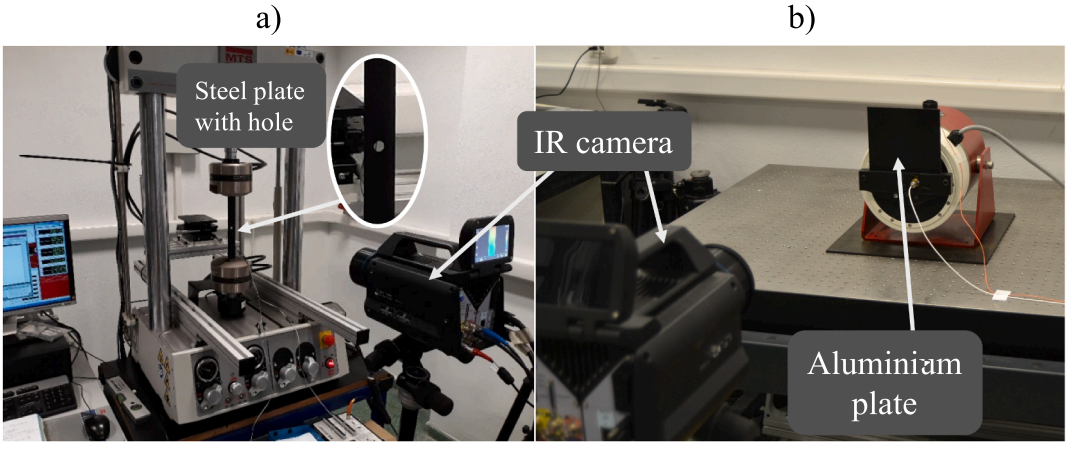


**Fig. 3.** Experimental setup for the thermal analysis of (a) a stress concentrator in a steel plate under axial loading and (b) the mode shapes of an aluminium plate under multi-harmonic excitation using IR vision technology.

### 3.2. Mode shapes

#### 3.2.1. Setup

In this experiment, the thermoelastic effect occurring at the resonances of a 2 mm thick aluminium plate is analysed. The plate was mounted on the armature of a shaker, model Data Physics GW-V55/PA300E, to be excited. One of the edges of the plate was clamped to it whereas the rest remains free. The shaker was set so that the motion was horizontal, and the plate stayed vertical, as shown in Fig. 3 (b). In that position, the plate was 149 mm wide and 129 mm high. The shaker generates a vibration through the axial motion of its armature according to a drive signal. A NI-6251 DAQ generated it as the superposition of harmonic signals whose frequencies and magnitudes can be defined. Namely, those frequencies were resonances of the plate, which define the dynamic behaviour and where the deformation is amplified. Exciting multiple resonances simultaneously is much less time-consuming than individually, but the load power is shared. Moreover, a higher number of frequencies of interest are available, being a simple way to obtain diverse independent fields to illustrate the capabilities of the methods.

#### 3.2.2. Natural frequencies identification

The preliminary identification of plate's resonances was required for its later thermal analysis. From a simple modal identification, a set of resonances were identified to build up the multi-harmonic signal of natural frequencies. It was performed in a single-input single-output test, using an accelerometer on the shaker's armature to register the excitation and another on the upper right corner of the plate's rear surface to monitor its response. The plate was excited with a white noise signal up to 3500 Hz. The drive signal generation and the measurement task were both performed by the vibration controller Spider 80X. From the resulting frequency response function, nine resonances were selected as local maxima. The accelerometer on the plate was not removed in the subsequent tests so as not to modify the dynamic behaviour after the identification.

#### 3.2.3. Multi-harmonic test

The modes of the plate, as well as for many mechanical systems and structures, occur at higher frequencies than for the habitual use of infrared thermography for TSA. Therefore, the thermal emission progressively decreases and just the intrinsic amplification of the deformation in resonances can compensate it moderately. Two factors are involved in that: first, the attenuation of the thermal signal produced by the coating, which depends on the driving frequency and the coating thickness [37–39]; second, the lower amplitude of deformation [16]. That led to exploit the power of the shaker to achieve a suitable signal. For this reason, the nine frequencies were grouped into two sets, performed separately, to distribute the power into fewer frequencies. The Group I included the first five natural frequencies whereas the Group II included the last four. The corresponding drive signals consisted of a multi-harmonic signal at those frequencies whose amplitude increased with frequency, according to Table 1, to compensate for the reduction of stresses with frequency.

For both tests, the frame ratio of the IR camera was set at 300 fps, the fastest at the maximum resolution. As the analysed frequencies are mostly over the Nyquist's frequency (half the frame rate), those were perceived as alias frequencies as a result of folding the spectrum at multiples of the Nyquist's frequency [40]. According to this, the alias frequencies can be predicted, as listed in Table 1. Both the low level of the thermal signal and the power distribution to multiple frequencies required a long sequence, as shown in a previous study [16]. Hence, the number of images in the sequence of both tests was 15,000. That study also emphasised the importance of the integration time feature in these tests because of the higher frequencies of analysis. It represents the period in which the sensor is receiving the radiation, so the longer it is, the clearer is the signal. However, a trade-off between speed and clearness has to be achieved since a non-accurate value might be obtained if the temperature rate over time is too fast. For Group I it was set at 500 μs and 200 μs for Group II. The shape of the plate allowed to take advantage of most of the field-of-view of the camera, except small gap of background around the plate. Therefore, they were cropped before processing to fit the plate shape and reduce the processing time. The resulting images size was 495 × 598 pixels.

The application of the periodogram averaging method was performed using 300 images per segment and 150 samples of overlap. This yielded a spectrum of 151 lines from 0 to 150 Hz with a frequency resolution of 1 Hz, according to the method's description. As can be observed, the original data was compressed with 1:100 ratio, retaining the meaningful information and accomplishing that all the excited frequencies (as their alias) exactly occurred at a frequency line. Again, no window was required. For lock-in correlation, the whole sequences of 15,000 images were processed. As the whole sequences lasted 50 s, they meet the condition of containing an integer number of periods of all the excited frequencies, particularly their alias.

Although the drive signal was actually measured during the experiments through the DAQ synchronised with the IR camera, a

**Table 1**
List of natural frequencies, and its amplitude in the drive signal, included in each group for multi-harmonic excitation of the aluminium plate.

| Group I | | | Group II | | |
|---|---|---|---|---|---|
| Frequency (Hz) | Alias frequency (Hz) | Drive signal amplitude (V) | Frequency (Hz) | Alias frequency (Hz) | Drive signal amplitude (V) |
| 122 | 122 | 0.25 | 1290 | 90 | 1.2 |
| 207 | 93 | 0.25 | 1420 | 80 | 1.0 |
| 561 | 39 | 0.5 | 1620 | 120 | 1.2 |
| 611 | 11 | 0.5 | 1885 | 85 | 1.5 |
| 787 | 113 | 2.0 | | | |

synthetic signal was created as the sum of sine functions of zero initial phase for the periodogram calculation. Likewise, the mono-harmonic signal for lock-in correlation was also created as a zero initial phase sine. As the same reference phase was again employed for both, it allowed checking the phase shift from both methods afterwards.

## 4. Results and discussions

### 4.1. Thermal maps

#### 4.1.1. Stress concentration

Resulting from the analysis of the stress concentrator, the images representing the sum of normal stresses were obtained for the two frequencies of interest: the loading frequency, 10 Hz, and its superharmonic, 20 Hz. They were complex images that include the information of the amplitude of the temperature variation and the phase shift. For lock-in correlation, they were the result of performing the correlation for each frequency individually, whereas, for the periodogram averaging method, they were obtained at the specific frequency line within the 151 lines spectrum.

Fig. 4 shows the left half of the maps obtained by each method. For illustration purposes, they are presented together in the same image, separated by a dashed line, to improve the comparison. This is possible thanks to the symmetry of the sample and the load and, thus, the symmetry of the thermal maps. On the left, the thermal distribution from lock-in correlation is shown, whereas the map from the periodogram is on the right. They represent the amplitude of the signal, where the phase was used to resolve the sign.

The map at 10 Hz shows the main behaviour of the plate, characterised by the well-known stress distribution near the concentrator. For 20 Hz, there is no load but the maps reveal a temperature variation at this frequency located where the stress intensification occurs. The information provided by the second harmonic map indicates that the thermal signal is not purely sinusoidal, i.e., it is distorted. Hence, the presence of non-linearities is revealed at this frequency, despite not being a valid map for thermoelastic analysis.

Regarding the method comparison, one of the first conclusion to be made from this result is that there is no difference in practice on using one method or the other. They show the same patterns with the same magnitude at both frequencies, including the most subtle details or noise. As can be observed, the level of the thermal signal at the loading frequency is greater than the typical sensitivity (about few mK), so long sequences were not required. Despite that, the sequence was longer than required for the loading frequency to reveal the non-linearities in the second harmonic. Therefore, this experiment entails a case for a low number of frequencies of interest and a short sequence of images, in comparison with the next experiment.

#### 4.1.2. Mode shapes

For the analysis of mode shapes in a plate, the symmetry of the geometry and load conditions yielded symmetric or antisymmetric thermal maps. Hence, the same strategy was followed to illustrate the result of the methods together. Fig. 5 show the maps for the frequencies in Group I and Fig. 6 for the higher frequencies of Group II. The phase of the reference signal for both methods was the

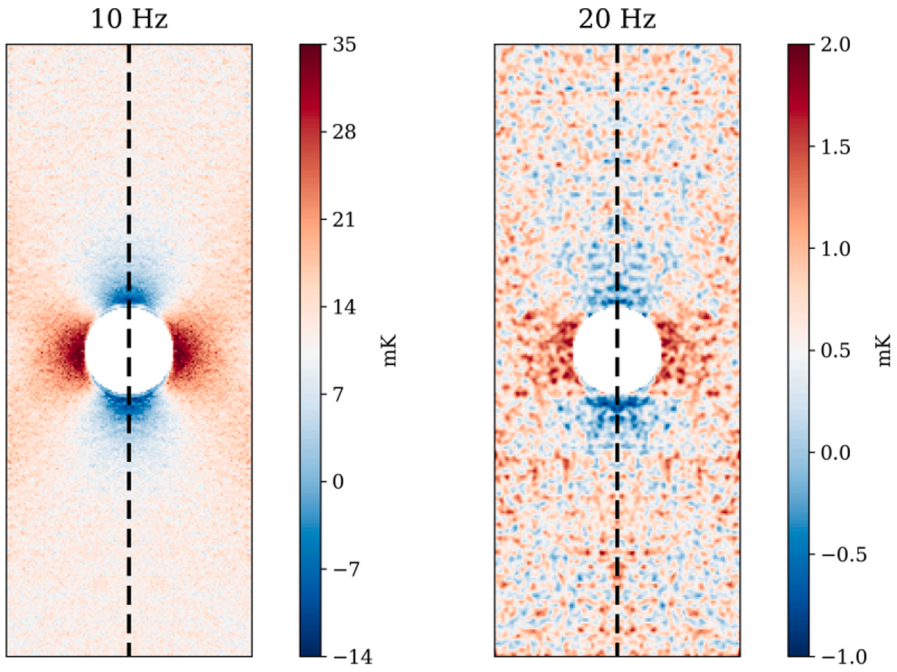


**Fig. 4.** Thermal maps of the concentrator analysis at the load frequency and its second harmonic. Separated by a dashed line, the left halves show the maps obtained by lock-in correlation and the right by the periodograms calculation.

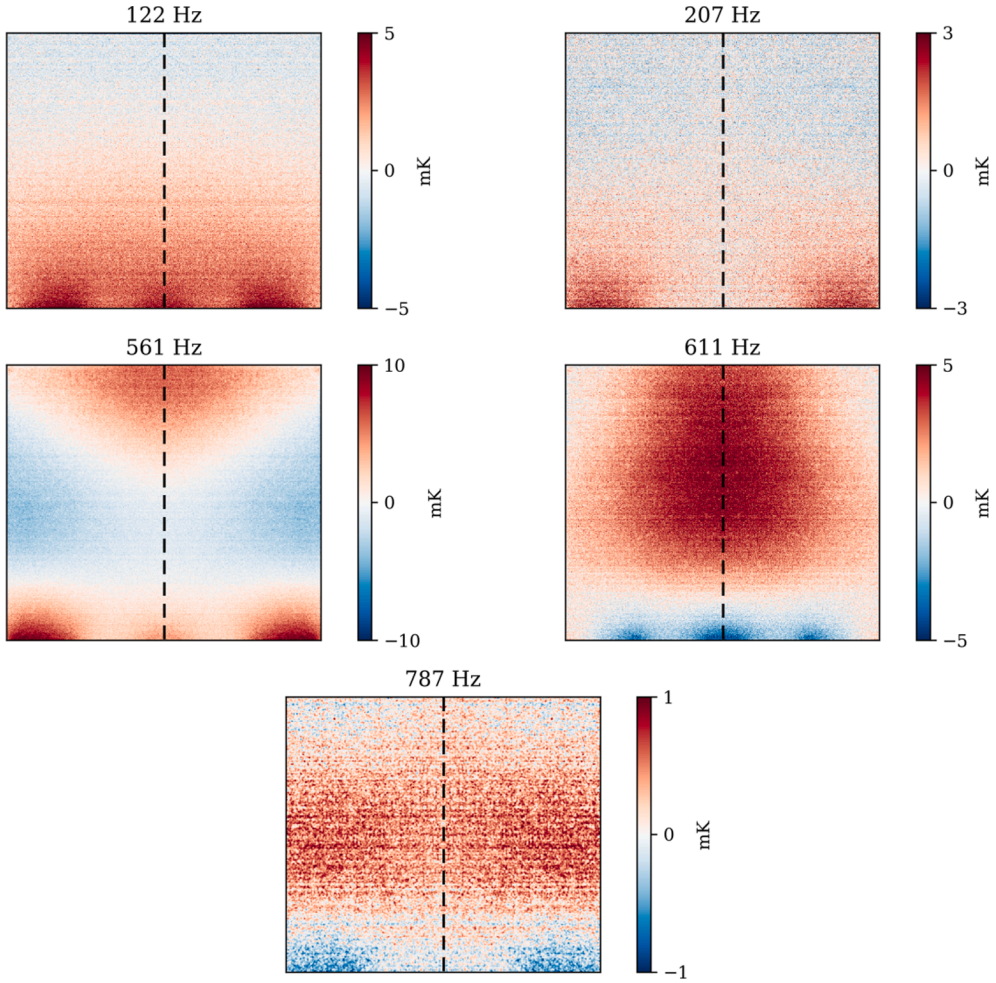


**Fig. 5.** Thermal maps of the mode shape analysis of the Group I test frequencies. Separated by a dashed line, the left halves show the maps obtained by lock-in correlation and the right by the periodograms calculation.

same, so the same phase was used to resolve the sign.

In these maps, the influence of the displacement and stresses level reduction with frequency is noticed in the thermal amplitude. The attenuation of the signal due to the paint coating also becomes important for the highest frequencies. Overall, they produce a noise increment with frequency, besides the influence of shorter integration times. The effect of the coating makes that the level of the thermal signal cannot be purely attributed to the plate stress field, but the shape is useful as a representation of modal shapes and the experiment still serves to assess both methods. Some modes, such as 207, 787, 1420 and 1885 Hz, are antisymmetric, so the combined representation of the same half from the two methods in Fig. 5 and 6 are not representative of the real shape. They were additionally provided in Fig. 7, where the antisymmetry can be observed. However, this kind of modes is typically noisier since antisymmetric shapes are hard to excite with a symmetric load. This is especially clear for the mode 1420 Hz, where the shape is hardly recognised.

The purpose of such an experiment is different from the former and some of its key characteristics are opposite. It provided a wider variety of independent maps at high frequencies with outstanding quality but the level signals are lower (just a few mK), which required long sequences to process. However, the comparison of these results yields the same conclusion: both methods are practically identical regarding the maps.

### *4.2. Computation efficiency*

After proving that the results of both methods are completely equivalent, or practically equal, using one or the other would depend on the computation efficiency. An evaluation of the processing time and the RAM consumption is presented in this section. Using the thermal sequences for both tests, the global computation time was registered by repeating 100 times the calculation through each method. Fig. 8 shows the resulting computation time for (a) the concentrator experiment and (b) the Group I experiment of mode shapes. The figure also indicates the mean value and the standard deviation in every case.

The main point to consider is the number of studied frequencies in each test. For lock-in, the total processing time depends on that

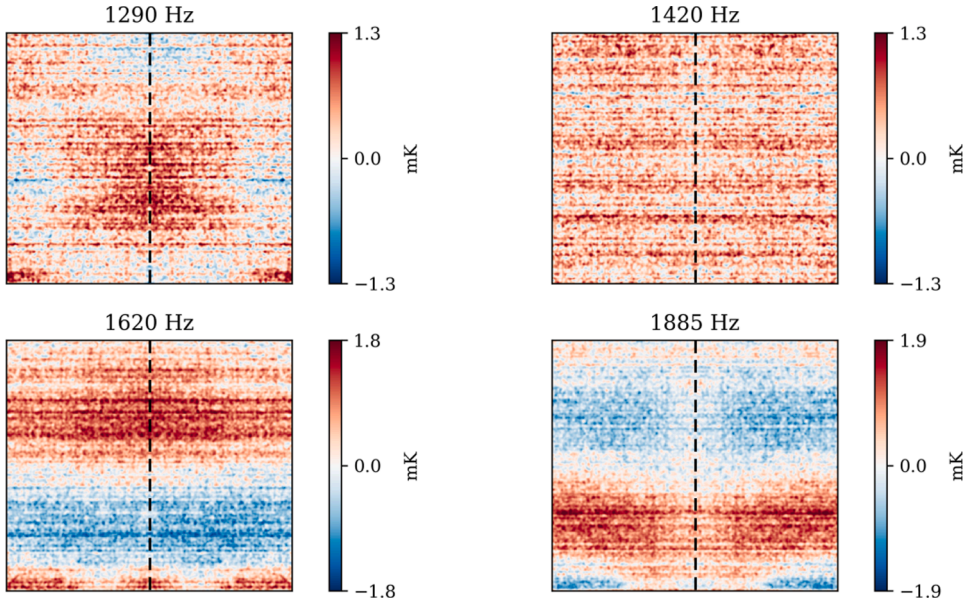


**Fig. 6.** Thermal maps of the mode shape analysis of the Group II test frequencies. Separated by a dashed line, the left halves show the maps obtained by lock-in correlation and the right by the periodograms calculation.

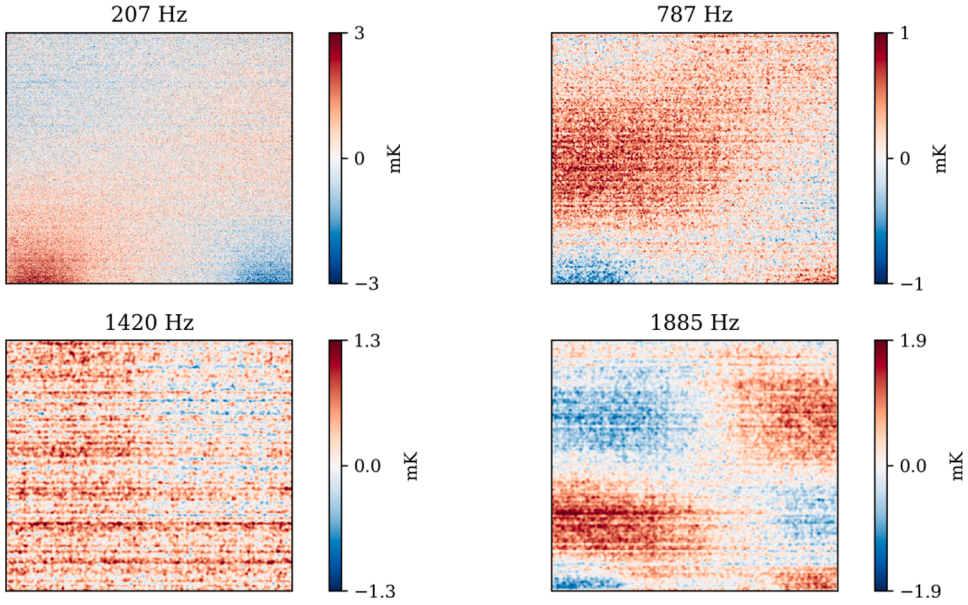


**Fig. 7.** Full thermal maps of the antisymmetric mode shapes obtained by lock-in correlation.

number, as the correlation must be performed for each frequency individually. However, it is indifferent for periodograms, where the whole set of frequency lines is provided simultaneously. According to the mean time for the computation of all the harmonics provided in Fig. 8, the average processing time per harmonic term in the concentrator experiment was 0.63 s for lock-in correlation and 3.75 s for the periodogram method. For the Group I of the mode shape analysis, it is 41.1 s per harmonic term for the periodogram method and 132.4 s for lock-in correlation. As expected, lock-in is faster in the concentrator experiment since the number of frequencies to analyse is low, and the contrary for the mode shape analysis as the number of frequencies increases. For Group II, the average time per mode would be the same for lock-in regardless the number of analysed modes, because the same parameters processing parameters were employed. However, the global time for the periodograms computation is expected to be the same, therefore analysing one less mode would increase the average time per mode to 51.4 s, which is still significantly shorter regarding lock-in.

Additionally, a relevant conclusion can be made from these results regarding the sequence length. It can be observed that, even if the number of frequencies in the concentrator experiment increased to five (to be comparatively equivalent to the modal experiment),

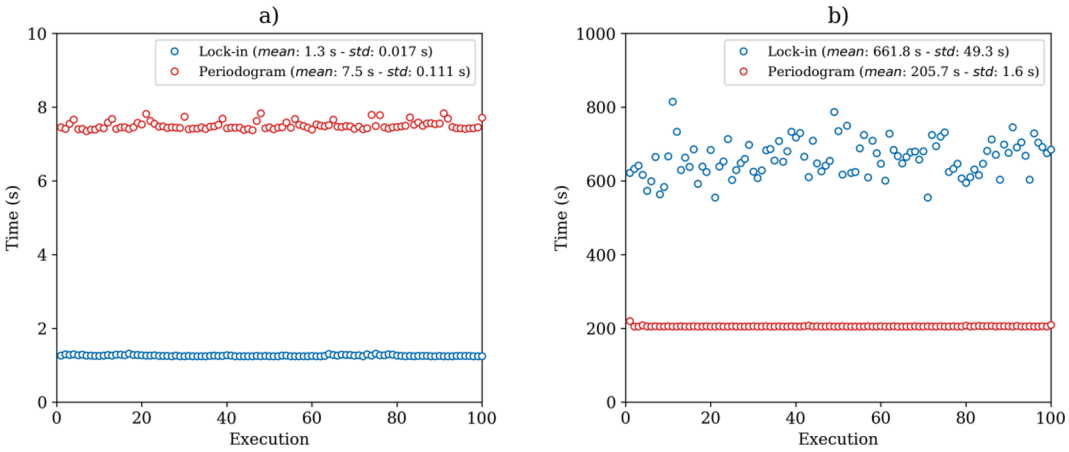


**Fig. 8.** Computation time for 100 executions using lock-in correlation and the proposed periodogram averaging method for (a) the concentrator and (b) the Group I modal experiment.

the assigned time to retrieve a harmonic in the periodogram method would be still higher than lock-in time per frequency, namely, 1.5 s. This would be contradictory to the previous conclusion without further considerations. As the same frame rate and processing parameters were employed for both tests, it revealed the sequence length as another determinant factor. The concentrator analysis was performed under a load that produced a high level of thermal emission at a low frequency. Thus, the sequence does not need to be long: 3 000 images were employed. On the contrary, the analysis of mode shapes involved significantly longer sequences, 15,000 images, as the thermal signal is much weaker due to the excitation procedure and the much higher frequencies. As the full sequence must be employed for lock-in computation whereas the periodogram method was performed with the same segment length (300 images) in both experiment, it can be unequivocally concluded that the length of the sequences increases the lock-in processing time relative to periodograms. Moreover, it is observed that the computation time using periodograms is much more stable for long sequences, as shown in Fig. 8 (b), with a standard deviation which is 0.8 % of the mean calculation time, whereas is 7.5 % for lock-in.

The RAM peak consumption during the processing revealed that it is about 2.22 times higher for lock-in. Although details on the computational problem are not provided here, it has to be considered that the computation of lock-in correlation according to eq. (12) involves the creation of a new array of the same size as the income thermal signals array. However, the periodogram method works with short segments of the income and, thus, the memory requirements are lower, especially for long image sequences.

Although the periodogram computation time depends on the chosen parameters, it can be shown that a modification of the parameters would not be convenient with regard to the results and the computation time. According to [36], the influence of the periodogram segments length, $L$, on the computation time is proportional to $\log_2 L$, considering that longer segments involve less segments to process and average. Overall, the segments length would not require a significant variation, as both experiments are quite characteristic TSA applications and it provides enough frequency resolution. As an example, if five times longer segments had been utilised, it would have just implied an increment of 28% of the computation time, and a 12% increment if the length was double, which is subtle or even negligible. However, the RAM consumption and the output data size would increase proportionally to the segment size. The overlap does affect the processing time since it increases the number of segments to average. Its influence is therefore inversely proportional, so a double overlap implies a 100% increment of the time. Nevertheless, the value here adopted is standard for most applications. The quality of the results prove that is enough compared to lock-in and a lower overlapping would reduce even more the processing time.

Finally, the periodogram averaging method is advantageous when the number of required thermal maps, at different frequencies, is unknown beforehand as it provides the whole spectrum at once. In the case of superharmonics analysis, it can be worked out by creating a signal with enough number of harmonics or, more generally, the real amplitude of all the lines in the spectrum can be efficiently achieved by creating a reference signal that contains all those terms. The latter can be also useful for the detection of terms not related to the load frequency and its superharmonics, or to provide the information about the noise in the signal. In both cases, the signal creation can be easily programmed without affecting the periodogram computation.

## 5. Conclusions

Regarding the lock-in correlation method and those based on Fourier transform for the analysis of thermoelastic signals, this work provides a thorough insight to reach important conclusions for practical situations. First, a new method has been proposed using the periodograms resulting from the averaged cross-power spectrum of the thermal and reference signals. It provides significant data compression without rejecting the relevant information of the signal regarding the simple Fourier transform. Moreover, it keeps the phase shift information avoiding signal cancellation, unlike the Fourier transform.

For the evaluation of the methods, two of the most representative uses of TSA have been performed. The two experiments involve opposite cases that highlight the capabilities of the methods. The results have clearly proved that there is no numerical difference

between methods, in terms of the resulting thermal maps. However, the computational efficiency evaluation has revealed significant differences. Therefore, it has been shown that lock-in is more efficient to analyse a low number of frequencies in short sequences, where the thermoelastic content is high in the thermal signal. That would be the case for fracture and fatigue analysis. On the contrary, the periodogram averaging method is more efficient for long sequences with a higher number of frequencies, for instance, in the multi-harmonic analysis of mode shapes. Essentially, lock-in provides concise information for the frequency of analysis but the periodogram averaging method is actually more complete, as contains the whole information of the spectrum of analysis including the noise distribution. Nevertheless, the periodogram averaging method is also advantageous regarding memory requirements due to working with short segments of the data. Finally, the sequential character of lock-in correlation requires a previous identification of the reference signal phase in multi-harmonic signals when the real phase shift is required, which is intrinsically obtained in the periodograms without further steps.

In conclusion, this comparative work contributes to advance towards a simpler, economical, versatile implementation of the off-line methods for TSA in multiple applications.

## CRediT authorship contribution statement

**A.J. Molina-Viedma:** Conceptualization, Methodology, Software, Validation, Formal analysis, Investigation, Data curation, Writing - original draft, Writing - review & editing. **L. Felipe-Sesé:** Conceptualization, Methodology, Validation, Investigation, Writing - original draft, Writing - review & editing. **E. López-Alba:** Conceptualization, Methodology, Resources, Writing - review & editing. **F. A. Díaz:** Conceptualization, Writing - review & editing, Supervision, Project administration, Funding acquisition.

## Declaration of Competing Interest

The authors declare that they have no known competing financial interests or personal relationships that could have appeared to influence the work reported in this paper.

## Acknowledgements

The authors gratefully acknowledge the financial support from the Spanish Government through the research project “Proyecto de Investigación de Excelencia del Ministerio de Economía y Competitividad” under grant number MAT2016-76951-C2-1-P and from the Andalusian Regional Government through the research project “Ayudas a proyectos de I+D+i (PAIDI 2020)” under grant number P20_00312, without which this work could not have been performed.

## References

[1] G. Pitarresi, E.A. Patterson, A review of the general theory of thermoelastic stress analysis, J. Strain Anal. Eng. Des. 38 (5) (2003) 405–417, https://doi.org/10.1243/03093240360713469.
[2] R.J. Greene, E.A. Patterson, R.E. Rowlands, Thermoelastic Stress Analysis, in: Springer Handb. Exp. Solid Mech., Springer US, Boston, MA, 2008: pp. 743–768. https://doi.org/10.1007/978-0-387-30877-7_26.
[3] S.T. Lin, J.P. Miles, R.E. Rowlands, Image enhancement and stress separation of thermoelastically measured data under random loading, Exp. Mech. 37 (3) (1997) 225–231, https://doi.org/10.1007/BF02317411.
[4] J.M. Dulieu-Smith, Alternative calibration techniques for quantitative thermoelastic stress analysis, Strain 31 (1995) 9–16, https://doi.org/10.1111/j.1475-1305.1995.tb00949.x.
[5] J. Gamot, T. Lasserre, L. Richard, J. Neggers, N. Swiergiel, F. Hild, Calibrating thermoelastic stress analysis with integrated digital image correlation: Application to fatigue cracks, J. Strain Anal. Eng. Des. 54 (5-6) (2019) 320–330, https://doi.org/10.1177/0309324719874924.
[6] A.L. Audenino, V. Crupi, E.M. Zanetti, Thermoelastic and elastoplastic effects measured by means of a standard thermocamera, Exp. Tech. 28 (2) (2004) 23–28, https://doi.org/10.1111/ext.2004.28.issue-210.1111/j.1747-1567.2004.tb00155.x.
[7] G. Pitarresi, L. D'Acquisto, A.M. Siddiolo, Thermoelastic stress analysis by means of an infrared scanner and a two-dimensional fast Fourier transform-based lock-in technique, J. Strain Anal. Eng. Des. 43 (6) (2008) 493–506, https://doi.org/10.1243/03093247JSA348.
[8] F.A. Díaz, J.R. Yates, E.A. Patterson, Some improvements in the analysis of fatigue cracks using thermoelasticity, Int. J. Fatigue 26 (2004) 365–376, https://doi.org/10.1016/j.ijfatigue.2003.08.018.
[9] A.S. Patki, E.A. Patterson, Thermoelastic stress analysis of fatigue cracks subject to overloads, Fatigue Fract. Eng. Mater. Struct. 33 (2010) 809–821, https://doi.org/10.1111/j.1460-2695.2010.01471.x.
[10] D. Chen, G. Li, Y. Wang, Q. Xiao, Research on fatigue crack propagation of a T-joint based on XFEM and TSA, Eng. Fract. Mech. 222 (2019) 106707, https://doi.org/10.1016/j.engfracmech.2019.106707.
[11] R.A. Tomlinson, A.D. Nurse, E.A. Patterson, On determining stress intensity factors for mixed mode cracks from thermoelastic data, Fatigue Fract. Eng. Mater. Struct. 20 (1997) 217–226, https://doi.org/10.1111/j.1460-2695.1997.tb00279.x.
[12] M. Zanganeh, R.A. Tomlinson, J.R. Yates, T-stress determination using thermoelastic stress analysis, J. Strain Anal. Eng. Des. 43 (6) (2008) 529–537, https://doi.org/10.1243/03093247JSA349.
[13] A. Chrysochoos, B. Berthel, F. Latourte, A. Galtier, S. Pagano, B. Wattrisse, Local energy analysis of high-cycle fatigue using digital image correlation and infrared thermography, J. Strain Anal. Eng. Des. 43 (6) (2008) 411–422, https://doi.org/10.1243/03093247JSA374.
[14] T.R. Emery, J.M. Dulieu-Barton, Thermoelastic stress analysis of damage mechanisms in composite materials, Compos. Part A Appl. Sci. Manuf. 41 (12) (2010) 1729–1742, https://doi.org/10.1016/j.compositesa:2009.08.015.
[15] A. Chrysochoos, V. Huon, F. Jourdan, J.-M. Muracciole, R. Peyroux, B. Wattrisse, Use of full-field digital image correlation and infrared thermography measurements for the thermomechanical analysis of material behaviour, Strain 46 (2010) 117–130, https://doi.org/10.1111/j.1475-1305.2009.00635.x.
[16] Á.J. Molina-Viedma, L. Felipe-Sesé, E. López-Alba, F.A. Díaz, Thermoelastic effect in modal shapes at high frequencies using infrared thermography, Measurement 176 (2021) 109180, https://doi.org/10.1016/j.measurement.2021.109180.
[17] N. Harwood, W.M. Cummings, eds., Thermoelastic Stress Analysis, IOP Publishing (Adam Hilger), Bristol (England), 1991.
[18] Javier Gaspar, Suei Feng Chen, Alejandro Gordillo, Mateo Hepp, Pablo Ferreyra, Carlos Marqués, Digital lock in amplifier: Study, design and development with a digital signal processor, Microprocess. Microsyst. 28 (4) (2004) 157–162, https://doi.org/10.1016/j.micpro.2003.12.002.

[19] John H. Scofield, Frequency-domain description of a lock-in amplifier, Am. J. Phys. 62 (2) (1994) 129–133, https://doi.org/10.1119/1.17629.
[20] G. Pitarresi, Lock-in signal post-processing techniques in infra-red thermography for materials structural evaluation, Exp. Mech. 55 (4) (2015) 667–680, https://doi.org/10.1007/s11340-013-9827-1.
[21] J.R. Estrada Estrada, E.A. Patterson, Path dependency in thermoelastic stress analysis, Exp. Mech. 44 (2004) 567–573, https://doi.org/10.1177/0014485104049395.
[22] D. Chen, S. Sun, J.M. Dulieu-Barton, Q. Li, W. Wang, Crack growth analysis in welded and non-welded T-joints based on lock-in digital image correlation and thermoelastic stress analysis, Int. J. Fatigue 110 (2018) 172–185. https://doi.org/10.1016/j.ijfatigue.2018.01.020.
[23] S.A. Grammatikos, E.Z. Kordatos, T.E. Matikas, A.S. Paipetis, On the fatigue response of a bonded repaired aerospace composite using thermography, Compos. Struct. 188 (2018) 461–469, https://doi.org/10.1016/j.compstruct.2018.01.035.
[24] X.D. Li, H. Zhang, D.L. Wu, X. Liu, J.Y. Liu, Adopting lock-in infrared thermography technique for rapid determination of fatigue limit of aluminum alloy riveted component and affection to determined result caused by initial stress, Int. J. Fatigue 36 (1) (2012) 18–23, https://doi.org/10.1016/j.ijfatigue.2011.09.005.
[25] J. Liu, J. Gong, L. Liu, L. Qin, Y. Wang, Investigation on stress distribution of multilayered composite structure (MCS) using infrared thermographic technique, Infrared Phys. Technol. 61 (2013) 134–143, https://doi.org/10.1016/j.infrared.2013.08.004.
[26] Takahide Sakagami, Yui Izumi, Shiro Kubo, Application of infrared thermography to structural integrity evaluation of steel bridges, J. Mod. Opt. 57 (18) (2010) 1738–1746, https://doi.org/10.1080/09500340.2010.511289.
[27] A. Di Renzo, R. Marsili, M. Martarelli, M. Moretti, G. Rosati, G.L. Rossi, Simultaneous application of scanning laser vibrometry and thermoelasticity for measurement of stress-strain fields on mechanical components, in: Seventh Int. Conf. Vib. Meas. by Laser Tech. Adv. Appl., Ancona, 2006: p. 63450H. https://doi.org/10.1117/12.693161.
[28] R K Fruehmann, J M Dulieu-Barton, S Quinn, J Peton-Walter, P A N Mousty, The application of thermoelastic stress analysis to full-scale aerospace structures, J. Phys. Conf. Ser. 382 (2012) 012058, https://doi.org/10.1088/1742-6596/382/1/012058.
[29] D. Backman, R.J. Greene, Gas turbine blade stress analysis and mode shape determination using thermoelastic methods, Appl. Mech. Mater. 13–14 (2008) 281–287, https://doi.org/10.4028/www.scientific.net/AMM.13-14.281.
[30] R. De Finis, D. Palumbo, U. Galietti, Mechanical behaviour of stainless steels under dynamic loading: An investigation with thermal methods, J. Imaging. 2 (2016) 1–17, https://doi.org/10.3390/jimaging2040032.
[31] F. Ancona, D. Palumbo, R. De Finis, G.P. Demelio, U. Galietti, Automatic procedure for evaluating the Paris Law of martensitic and austenitic stainless steels by means of thermal methods, Eng. Fract. Mech. 163 (2016) 206–219, https://doi.org/10.1016/j.engfracmech.2016.06.016.
[32] F.A. Díaz, J.M. Vasco-Olmo, E. López-Alba, L. Felipe-Sesé, A.J. Molina-Viedma, D. Nowell, Experimental evaluation of effective stress intensity factor using thermoelastic stress analysis and digital image correlation, Int. J. Fatigue 135 (2020) 105567, https://doi.org/10.1016/j.ijfatigue.2020.105567.
[33] M L Silva, G Ravichandran, Combined thermoelastic stress analysis and digital image correlation with a single infrared camera, J. Strain Anal. Eng. Des. 46 (8) (2011) 783–793, https://doi.org/10.1177/0309324711418286.
[34] M.L. Silva, G. Ravichandran, Stress field evolution under mechanically simulated hull slamming conditions, Exp. Mech. 52 (1) (2012) 107–116, https://doi.org/10.1007/s11340-011-9529-5.
[35] Giuseppe Pitarresi, Riccardo Cappello, Giuseppe Catalanotti, Quantitative thermoelastic stress analysis by means of low-cost setups, Opt. Lasers Eng. 134 (2020) 106158, https://doi.org/10.1016/j.optlaseng.2020.106158.
[36] P. Welch, The use of fast Fourier transform for the estimation of power spectra: A method based on time averaging over short, modified periodograms, IEEE Trans. Audio Electroacoust. 15 (2) (1967) 70–73, https://doi.org/10.1109/TAU.1967.1161901.
[37] J. McKelvie, Consideration of the surface temperature response to cyclic thermoelastic heat generation, Stress Anal. Thermoelastic Tech. 0731 (1987) 44, https://doi.org/10.1117/12.937886.
[38] A.K. Mackenzie, Effects of surface coatings on infra-red measurements of thermoelastic responses, Stress Vib. Recent Dev. Ind. Meas. Anal. 1084 (1989) 59, https://doi.org/10.1117/12.952906.
[39] C.S. Welch, M.J. Zickel, Thermal coating characterization using thermoelasticity, Rev. Prog. Quant. Nondestruct. Eval. 12 (1993) 1923–1930, https://doi.org/10.1007/978-1-4615-2848-7_247.
[40] Y. Yang, C. Dorn, T. Mancini, Z. Talken, S. Nagarajaiah, G. Kenyon, C. Farrar, D. Mascareñas, Blind identification of full-field vibration modes of output-only structures from uniformly-sampled, possibly temporally-aliased (sub-Nyquist), video measurements, J. Sound Vib. 390 (2017) 232–256, https://doi.org/10.1016/j.jsv.2016.11.034.